Computer simulation of excitation conductivity by qubit model*

Yuri I. Ozhigov, Nikita A. Skovoroda

Lomonosov Moscow State University, Faculty of Computational Mathematics and Cybernetics, Moscow, Russia

We describe the computational model of quantum energy transfer in JCH like chains based on qubit representation of quantum states. The chain consists of optical cavities, each of which contains one two level atom interacting with field inside the cavity. Photons can jump between cavities that creates the effect of conductivity in the chain. Mathematical model of the conductivity is based on the qubit representation of quantum states in which any qubit has the fixed physical sense. This allows to include the dephasing noise, input and output intensity and analyse the contra intuitive quantum effects like dephasing assisted transport (DAT) and quantum bottleneck. The program realization of the model is based on the package Mathematica and utilizes such advantages of object oriented programming as module structure of the program. We represent the results of numerical simulation: the optimal output and input intensities, DAT and bottleneck.

1. Introduction and background

Computer simulation is the important tool for the investigation of open quantum systems (see [1]), because their dynamics rarely has analytical representation. The description of intriguing purely quantum effects, like DAT or bottleneck, requires sufficiently large dimensionality of Hilbert space of quantum states. The extremal manifestation of this complexity are the fast quantum algorithms, which can outperform their classical counterparts for the mathematical tasks of the search type (Grover search algorithm, Shor integer factoring). The simulation on classical computers thus requires rigid economy of computing resource that are of our disposal: the memory.

It is convenient to measure the memory in terms of bits; for the quantum states it will be qubit memory. For the classical simulation with n qubits we must store 2^n bits, and this value grows so fast that for the simulation on personal computers we are limited by the value $n = 12$, for supercomputers the values $n \approx 30$ are only accessible now and up to $n = 60$ in the foreseeable future. The supercomputer simulation is effective if only we can select carefully very limited computational task; to find the statement of such a task we should fulfil preliminary simulation on the more flexible personal computers, for which the preparation and tuning of the program is substantially easier.

In addition, even the usage of a supercomputer for the simulation of quantum dynamics requires the peculiar algorithms substantially optimizing the standard technique of linear algebra that can be found only in the framework of one ten of qubits, where the Hamiltonian matrix is in principle visible.

In this work we propose the qubit model, in which any qubit has the fixed physical sense. For example, if we encode the state of the single two level atom in the optical cavity in three qubits, we can reserve the first qubit for its state: $|0\rangle_1$ — ground, and $|1\rangle_2$ — excited, and the rest two qubits — for the state of the field, such that $|00\rangle_{2,3}$, $|01\rangle_{2,3}$, $|10\rangle_{2,3}$, $|11\rangle_{2,3}$ encode vacuum state, one, two and three photon states correspondingly. This approach makes possible to measure exactly the memory that we reserve for quantum states and manipulate it as it is convenient for the different forms of the model.

We will describe the qubit form of Jaynes-Cummings-Hubbard model (see [22, 23]), for the

*The work is supported by Russian Foundation for Basic Researches, Grant 15-01-06132 A.

chain of optical cavities, connected by optical fibres. Each cavity contains one atom with two energy levels: ground and excited that can interact with the field inside the cavity. Photons can also jumps from one cavity to the neighbouring with the fixed amplitude that creates the energy transport along the chain.

The cavity stores the photons of the fixed frequency ω_c close to the atomic frequency that creates the condition of valuable coupling between atoms and field. Fock states of the photons can be also used as the logical states for the quantum computer; this scheme has been proposed in the works [25, 26] and elaborated in the works [28–35]. The states of field can be effectively stored in the states of atomic ensembles (see, for example, [27]) that could help the initialization of a quantum computer.

We measure the effectiveness of the transport by the conductivity of excitations, that is the time in which the excitation travels from the beginning of the chain and reaches the end. We fix this time by the additional qubit called a sink, which interaction with the last cavity is irreversible. We also consider the noise, which affects conductivity in the form of dephasing that brings the interesting and practically important effect of increasing conductivity with the growth of the noise intensity: dephasing assisted transport — DAT (see the works [11,12,18–21], in which DAT is investigated in more details; in [36] one can find the treatment of conductivity in noiseless chains).

The conventional mathematical representation of such open quantum systems is Markov master equation in the form of Kossakowski-Lindblad (see [2] and [3]), which is applicable to the systems, which environment has no memory (however, in some important processes the environment has the memory, the main example is the process of life; the consideration of non Markovian processes can be found, for example, in [4], see also [5]). The influence of environment is typically treated as the source of decoherence, though it can create the interesting quantum effects, like quantum Zeno effect, in which the measurements helps to conserve the needed quantum state (see the works [6, 7]). The special noise can even suppress decoherence ([8]; see also the work [9] — the noise smoothing by a unitary control).

The influence of noise is very important for the conductivity in JCH chains — in artificial devices as well as in living organisms (see [10–12]).

The conductivity of a single excitation can be formulated in the form of quantum walks ([10, 13–16]).

DAT effect was investigated in details in the works [11, 12, 18–21] and others; this interest has arisen due its role in the light harvesting Fenna-Matthews-Olson (FMO) complex in green sulfur bacteria (see [17]).

Here we use excitation conductivity as the field of application of programming complex based on qubit approach. In the next section we explain the mathematical model, then we describe the computer program, and show the result of simulation made on working stations. In the last section we briefly discuss the results and perspectives.

2. Quantum effects in the energy transfer

We give a definition, starting with the most detailed model "excitations, photons, phonons." We consider a linear chain consisting of identical optical cavities with two level atoms inside. Each cavity holds the photons with frequency ω_c. Fock state with n photons inside i-th cavity we denote by $|n\rangle_{fi_i}$. Inside each i-th cavity there is one two-level atom, which eigenstates: ground and excited we denote by $|0\rangle_{at\ i},\ |1\rangle_{at\ i}$ correspondingly. The difference between frequencies of these states (detuning) $d = \omega_c - \omega_a$ is small in comparison with each of them: $d \ll \omega_c$ that allows to use rotating wave approximation for the atom-photon interaction at the large enough time frame, and Jaynes -Cummings model (JC). In addition, each atom is placed in a bath of thermal phonons that have dephasing effect on its excitation. In this paper all phonons have the same frequency ω_p, for which DAT effect is maximal. In fact, this frequency is equal to

the difference between eigen frequencies of the Hamiltonian of JCH model (see below) that are responsible for the transfer of excitations (see the work [12]).

The transfer of energy from the cavity to cavity occurs through the flight of photons between the cavities where $-\frac{1}{h}\delta_{i,j}$ is the amplitude of the flight from the cavity j to the cavity i per unit of time, so that the amplitudes of the opposing flights are mutually conjugate, that is $\delta_{i,j} = \bar{\delta}_{j,i}$.

The Hamiltonian of our model is thus obtained by adding to the Jaynes-Cummings Hubbard Hamiltonian H_{JCH} the term of exciton-phonon interaction $H_{int\ ep}$:

$$\begin{aligned} H = \quad & H_{JCH} + H_{int\ ep}, \\ & H_{JCH} = h\omega_a \sum_i \sigma_i^+ \sigma_i + h\omega_c \sum_i a_i^+ a_i + \sum_i (\gamma a_i^+ \sigma_i + \bar{\gamma} a_i \sigma_i^+) + \sum_{i \neq j} (\delta_{i,j} a_i^+ a_j + \bar{\delta} j, i a_j^+ a_i), \\ & H_{int\ ep} = g \sum_i (b_i^+ + b_i) \sigma_i^+ \sigma_i. \end{aligned} \tag{1}$$

Here a_i^+, a_i denote operators of creation and annihilation of a photon in i-th cavity, b_i^+, b_i^+- denote creation and annihilation of a phonon in i-th cavity, σ_i^+, σ_i- denote creation and annihilation of the excited state of the corresponding atom (excitation), γ is the amplitude of photon emitting by excited atom in the unit of time. We assume that the photon jump is possible between the neighbouring cavities only where it occurs with the same amplitude so that all $\delta_{i,j} = 0$ for $|i-j| \neq 1$, and for $|i-j| = 1$, $\delta_{i,j} = \delta$. Constant g is the intensity of exciton-phonon interactions (square root of Huang-Phys factors).

In the simplified model, which we call "excitation-phonon" photons are ignored, and excitations are transmitted from one atom to the other; its Hamiltonian H_{ep} has the form

$$H_{ep} = H_e + H_{int\ ep},\ H_e = h\omega_a \sum_i \sigma_i^+ \sigma_i + \sum_{i \neq j} (\mu_{i,j} \sigma_i^+ \sigma_j + \bar{\mu}_{j,i} \sigma_j^+ \sigma_i), \tag{2}$$

The inflow of the energy can be viewed either as a constant occurrence of the excitation on the first node, taking the energy income from the outer bath, or simply set the initial state of the first atom as excited, regardless of photons. In the first case the bath inflows can create excitation irreversibly, or we can simply consider the initial state of a strongly excited field in the first cavity, which interacts with the first atom.

There are two ways for the simulation of dephasing as well. Either we consider it as the interaction with the explicit phonons, or as the irreversible process with only excitations and without explicit phonons.

Combining all of the above methods of studying the conductivity, we get all kinds of particular computing models. In any case, for the irreversible models master equation of Kossakowski-Lindblad should be applied:

$$\begin{aligned} & U_{\delta t} = e^{-\frac{i \cdot \delta t}{\hbar} H}, \\ & \tilde{\rho}_{t+\delta t} = \delta t \sum_i (L_i \rho L_i^* - \frac{1}{2}(L_i^* L_i \rho + \rho L_i^* L_i)), \\ & \rho_{t+\delta t} = U_{\delta t}^* \tilde{\rho}_{t+\delta t} U_{\delta t}. \end{aligned} \tag{3}$$

which contains the unitary dynamics $U_{\delta t}$ as the particular case. Here Lindblad operators L_i describe the irreversible part of the process. For example, the irreversible runoff of excitations to the sink from the last node (end) is expressed by the operator $L_{sink} = g_{sink} |0\rangle_{end} |1\rangle_{sink} \langle 0|_{sink} \langle 1|_{end}$, where the positive coefficient g_{sink} expresses the intensity of runoff, dephasing in i-th node resulted from the interaction with the implicit phonons is reflected by the operator $L_{deph,\ i} = \sigma_i^+ \sigma_i$, photon leak through the walls of the i-th cavity — by $L_{det,\ i} = a_i$, etc.

We consider the resulting quantum effects of excitation conductivity. We determine the conductivity by the degree of filling sink in a certain time.

1). Quantum bottleneck. Reduction of conductivity with increasing intensity of the runoff. Graph of conductivity depending on the rate of the runoff is not monotonically increasing as would be in the case of classical conductivity, but has a local maximum at a finite rate g^0_{sink}. The nature of this counter-intuitive effect is purely quantum.

It can be explained by considering the dynamics of the population of the initial state according to the time when the runoff intensity is large. If there is no runoff, the dynamics will be similar to the graph of the cosine, which has a maximum point at the initial time. The runoff constantly destroys the excitation at the end of the chain that makes the density matrix close to the initial state in which a reduction of the excitonic population at the first atom decreases with time very weak. This process competes with the obvious classic excitonic population decrease with increasing runoff.

If the runoff is strong enough, it constantly holds the density matrix (and hence population of excitations in the first atom) in the initial state in which there is practically no reduction of excitonic population at all that results in " freezing " of the population, like in quantum Zeno effect, in which the effect of " freezing " comes from frequent measurements of the quantum state. In the case of the classical conductivity instead of cosine fall of excitonic population we would have a linear decrease, and there would be no bottleneck.

2). Dephasing assisted transport — DAT. A plot of the conductivity on the intensity of the noise (the number of phonons of the resonant frequency, or intensity of the interaction between excitations and phonons, expressed in coefficients of Lindblad for dephasing) has a local maximum at a non-zero point. This means that there is some non-zero noise intensity at which the conductivity is maximal. There are quantum processes, connected with the conductivity, the effectiveness of which is enhanced with the increase of noise, for example, mixing at random walks on graphs ([37]). Effect of DAT stands out among them due a special role it plays in biology.

DAT as a purely quantum effect. Dephasing is direct suppression of the off-diagonal elements of the density matrix. Quantum dynamics is obtained by adding the amplitude states, the evolution of which leads to the same point of the classical space. Dephasing shifts the phase of the amplitude to a certain area. If this area would be narrower than the natural spread of the phase of states in the absence of dephasing, this influence will make the interference more constructive, thus increasing conductivity. This effect can be illustrated by the example of road traffic. If possibilities of cars are the same and allow rapid acceleration and braking, then synchronous mode of motion (phase conservation) will support high bandwidth of the road. But if the possibilities of vehicles are very different, then to increase bandwidth it is needed to the contrary, smooth mode of braking and acceleration, i.e. dephasing.

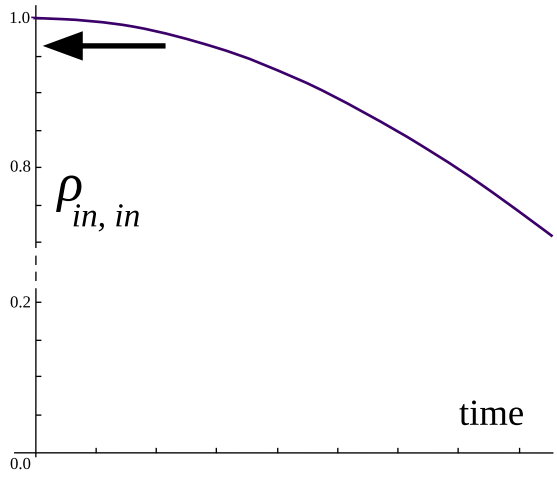

Figure 1. Dynamics of the population of the initial state with a large runoff intensity. Runoff shifts the density matrix to the initial state, the population of excitation in the first atom (for two-atom chain this is $\rho_{in,in}$) is shifted to the maximum point, and remains almost constant for a long time, preventing the sink filling.

3. Qubit-based model

3.1. Evolution equations

Kossakowski–Lindlbad equation in diagonal form is used for calculating non-unitary evolution:

$$i\hbar\frac{\partial\rho}{\partial t} = [H,\rho] + i\sum_{i}^{N^2-1}\gamma_i(A_i\rho A_i^* - \frac{1}{2}(A_i^*A_i\rho + \rho A_i^*A_i)) \tag{4}$$

Unitary evolution is optimized by diagonalizing the Hamiltonian.

In both cases, the evolution operator is determined by a Hamiltonian H with a set of non-normalized matrices $L_i = \sqrt{\gamma_i}A_i$.

For general (non-unitary) case, the evolution is computed by the equations (3) directy.

These evolution equations, as well as the measurement implementation, are independent of the used model. Various models could be created by constructing a Hamiltonian H and a set of Lindblad matrices L_i according to that model rules and semantics.

3.2. Qubit-based model construction

In order to allow simple operator-based constructing of Hamiltonians and Lindblad matrices we build the models by binding one a several qubits (a qubit group) to a specific state parameter, for example to the excitation of the first atom (see [38]). The model construction methods work with virtually huge matrices: for example for a chain of one-levelled excitons of a length 100, it would have a virtual Hamiltonian of size $2^{100} * 2^{100}$ (one qubit per each exciton). If excitations were four-levelled, that would make two qubits for each excitation. These matrices are not actually constructed in memory, an energy-limiting projection is used which selects only those states that have the energy between the specified lower and upper bounds. The resulting Hamiltonian and Lindblad matrices which are used in the actual calculation have much smaller sizes due to this projection.

3.3. A chain of excitation-photon-phonon cavities

A general chain model was constructed. This model implements a chain of cavities, each of which has similar multi-level excitation, photon field, and phonons. It has energy limiting support and supports attaching an input source and an output sink.

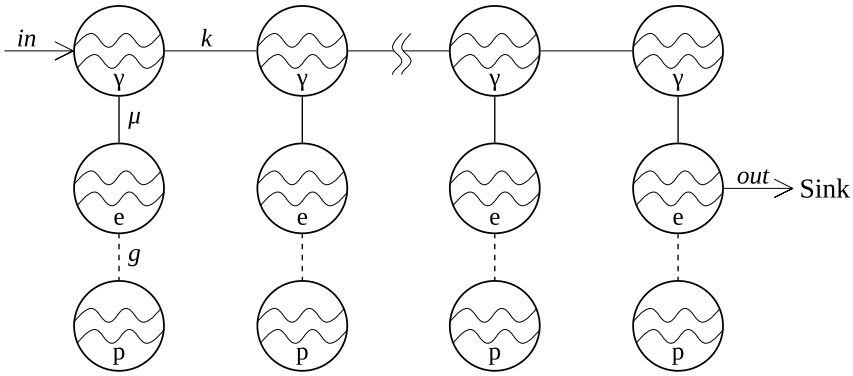

Figure 2. The exciton-photon-phonon cavities chain schematics.

There are three types of qubit groups in the chain:

- b_i is the phonon state for atom i, 1 — the corresponding phonon is present, 0 — the corresponding phonon is absent;
- a_i is the exciton state for atom i, 1 — excited state, 0 — not excited;
- p_i is the photon state for atom i, 1 — there is a photon, 0 — no photon.

The chain model has the following parameters:

- N_{atoms} — the number of atoms,
- k — photon tunnelling rate between neighbouring cavities,
- μ — photon–atom interaction strength,
- g — phonon–atom interaction strength,
- ω_a — frequency of one excitation (atomic transition frequency),
- ω_p — frequency of one photon (cavity frequency),
- ω_g — frequency of one phonon,
- in — input rate, replenishment coefficient for the first excitation a_1,
- out — output rate, sink coefficient for transferring excitation from $a_{N_{atoms}}$ to s.

Hamiltonian of the system equals to Jaynes–Cummings–Hubbard Hamiltonian:

$$\begin{aligned} H = &\sum_i \omega_p p_i^+ p_i^- + \sum_i \omega_a a_i^+ a_i^- + \sum_i \omega_b b_i^+ b_i^- + \sum_i (k p_{i+1}^+ p_i^- + k^* p_i^+ p_{i+1}^-) + \\ &\sum_i (\mu p_i^- a_i^+ + \mu^* p_i^+ a_i^-) + (g + g^*) \sum_i ((b_i^- + b_i^+) a_i^+ a_i^-). \end{aligned} \tag{5}$$

The sink s is attached to the last exciton in the chain. Input and output is performed using Lindblad operators:

$$\begin{aligned} L_{in} &= in * p_1^+ \\ L_{out} &= out * s^+ p_{N_{atoms}}^- \end{aligned} \tag{6}$$

In all the follow-up graphs and results, it is taken $\omega_a = \omega_p = 0.1$ and $\omega_g = 0.01$.

3.4. Dephasing models

Two dephasing models were implemented:

- Unitary-based: with explicit phonons as shown on 2.
  Hamiltonian of the system has the $(g + g^*) \sum_i ((b_i^- + b_i^+) a_i^+ a_i^-)$ part.
- Lindblad-based: there are no explicit photons in the system. Hamiltonian of the system does not have the corresponding part, Lindblad-like dephasing operators $D_i = p_i^+ p_i^-$ are used instead [11].

With the addition of Lindblad-like dephasing operators, evaluation equation 3 takes the following form:

$$\begin{aligned} &\tilde{\rho}_{t+\delta t} = \delta t \sum_i (L_i \rho L_i^* - \frac{1}{2}(L_i^* L_i \rho + \rho L_i^* L_i)) + \delta t \sum_i d_i (D_i^* D_i \rho D_i^* D_i - \frac{1}{2}(D_i^* D_i \rho + \rho D_i^* D_i)), \\ &\rho_{t+\delta t} = U_{\delta t}^* \tilde{\rho}_{t+\delta t} U_{\delta t}. \end{aligned} \tag{7}$$

Here d_i are the coefficients of the corresponding dephasing operators. In this model, all of d_i are equal to g.

4. Implementation details

The above-described model was implemented using the Wolfram Mathematica computer algebra system, and was split into several modules, and the most important of them are *QuantumSystem*, *QuantumExperiment*, *QuantumMeasures*, and the models modules (one module for each model). For this work the corresponding model module was called *QuantumModelJCHqUni*. Those four modules would be referenced as *System*, *Experiment*, *Measures*, and *ModelJCH* below.

Figure 3 shows the relationships between the modules in the system, with *Experiment.nb* being the main notebook file with all the parameters and output. Dotted lines represent internal dependencies, solid lines represent the data flow.

Some micro-optimization details are discarded to simplify the description.

4.1. The model representation and the *ModelJCH* module

As shown above, the model could be fully described using a Hamiltonian H and set of Lindblad-like dephasing operators with corresponding coefficients: $\{(L_i, l_i)\}$ and $\{(D_j, d_j)\}$. The model is internally represented as a list of three elements:

- The description of the model and its parameters. For *ModelJCH*, stores the number of possible particles in the system. Not used in computation, could be of any type;
- Hamiltonian H of the system — a square two-dimensional list of complex numbers;
- A list of Lindblad-based operators, each of which is by itself a list of three elements:
  - The type of the operator, being either "*Lindblad*" or "*Dephasing*" — a string;

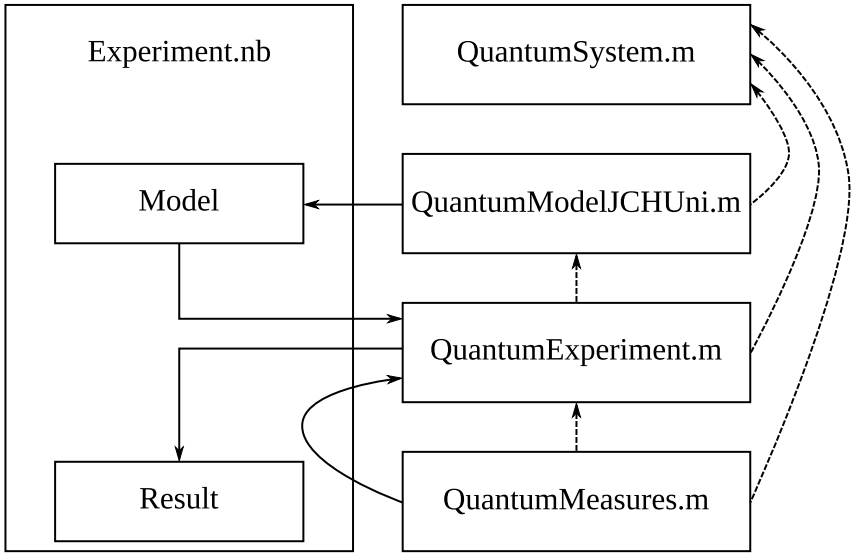

Figure 3. The relationships between modules.

- The coefficient l_i or d_i, depending on the type — a complex number. This one is optional, if the list has only two items, the coefficient is taken as being equal to 1;
- The matrix L_i or D_i, depending on the type — a square two-dimensional list of complex numbers with the same size as H.

The $ModelJCH$ module constructs such an list using the supplied parameters of the model and the helper functions from the $System$ module.

4.2. The *Experiment* module: QuantumExperiment function

The *Experiment* module contains everything related to the evolution logic, the most used exported function is *QuantumExperiment*.

QuantumExperiment method accepts one mandatory argument *system* — the model representation in the form mentioned in takes the model representation as described in 4.1, and some named optional arguments (*OptionsPattern*): *initialState*, *evolution*, *maxT*, *dT*, *plotStep*, *measure*, *criteria*, *return*.

initialState describes the initial state of the system, it is either a state vector number from the basis (from 1 to N, where $N * N$ is the size of the Hamiltonian), a state vector of length N, or a density matrix (two-dimensional list of size $N * N$). There is no future difference between passing in a number of some state vector or the corresponding state vector itself (for example, 2 corresponds to $\{0, 1, 0, ..., 0\}$).

evolution is the string that selects the numeric method for evolution, one of "*unitary*", "*eigen*", "*measurement*", and "*lindblad*", or a method that returns an evolution function itself. Those methods will be described below.

maxT is the total time of emulation, *dT* is the step time (δt). In an ordinary case, $\frac{maxT}{dT}$ is the maximum number emulation steps. *plotStep* is the number of emulation steps between the measurements. For an optimized evolution method that implements an accurate analytical solution (at the moment only the "*eigen*" method for the unitary evolution), *plotStep* has the effect of *dT* multiplier, where the effective dT_e is equal to $dT * plotStep$, and the maximum number of emulation steps is equal to $\frac{maxT}{dT * plotStep}$.

measure is either a string "*diagonal*" or "*entropy*" or a measurement function, that accepts

either one (current density matrix R) or two (current density matrix R and a density matrix R_{prev} of the previous step) arguments.

criteria accepts a function of one argument — the current density matrix R. If *criteria* is specified, the evolution stops on the step when the passed function returns $True$.

return is a string that describes what the method should return: "$measures$" — the list of measurements results, "$plot$" — either two- or three-dimensional plot of the measurements results (depends on whether the measurement returns a scalar or a vector), "$last$" — the final density matrix R, "$lastMeasure$" — the measurement result on the final density matrix, "$time$" — the total evolution time (for use with *criteria*), or "$time, lastMeasure$" — a list of two elements: the total evolution time and the measurement result on the final matrix.

4.3. The *Experiment* module: the emulation methods

The *evolution*, *system*, dT, and *initialState* arguments are passed to the internal *QuantumEvolution* method.

This method is designed to return an iteration function that performs the next step of the evolution and returns a density matrix.

If *evolution* is not a string, but is a function — the method returns $evolution[system, dT, initialState]$.

For all the built-in function, the output matrix is normalized with $M = (M + M^*)/2$ and $M = M/Trace[M]$ to partially eliminate the effect of inaccurate number representation.

evolution = "*unitary*" returns the most simple method $R_{t+\delta t} = U \cdot R_t \cdot U^*$, where $U = e^{-\frac{i \cdot \delta t}{\hbar} H}$. Lindblad-based part is discarded.

evolution = "*eigen*" returns a method similar to "*unitary*", but does not use an iterative algorithm and instead computes everything from the start. If the *initialState* is not a density matrix, this method could be expressed as:

$$\begin{aligned} V_t &= ER \cdot DiagonalMatrix[EU^n] \cdot ES \\ R_t &= V_t \cdot V_t^* \end{aligned} \tag{8}$$

Where V_t is the current state vector, EU is a vector of $EU_j = e^{-\frac{i \cdot \delta t}{\hbar} \lambda_j}$, $\{\lambda_j\}$ is the vector of eigenvalues of H, ES is the set of eigenvectors of H, V_0 is the initial state vector, $ER = V_0 \cdot ES^-1$, n is the number of step from 1.

The evolution of a density matrix has a similar, but has more computational operations.

evolution = "*measurement*" implements the following equations:

$$\begin{aligned} Ra_t &= R_{t-\delta t} + R_{t-\delta t} * C + C \cdot R_t + \sum_j XA_j \cdot R_{t-\delta t} \cdot XB_j \\ R_t &= U \cdot Ra_t \cdot U^* \end{aligned} \tag{9}$$

Matrices A_j, B_j, and C could be easily computed from the sets $\{L_i, l_i\}$ and $\{D_i, d_i\}$:

$$\begin{aligned} A_{li} &= L_i \\ B_{li} &= dT \cdot l_i \cdot L_i^* \\ A_{di} &= D_i^* \cdot D_i \\ B_{di} &= dT \cdot d_i \cdot D_i^* \cdot D_i \\ C &= -\frac{1}{2} dT \left(\sum_i l_i \cdot L_i^* \cdot L_i + \sum_j d_j \cdot D_j^* \cdot D_j\right) \end{aligned} \tag{10}$$

evolution = "*lindblad*" implements the following equations:

$$
\begin{aligned}
S_t &= S_{t-\delta t} + AN_{t-\delta t} \cdot (\sum_j XA_j \cdot R_{t-\delta t} \cdot XB_j) \cdot AN^*_{t-\delta t} \\
AN_t &= ANd \cdot AN_{t-\delta t} \\
AP_t &= APd \cdot AP_{t-\delta t} \\
R_t &= AP_t \cdot S_t \cdot AP^*_t
\end{aligned}
\tag{11}
$$

Where

$$
\begin{aligned}
AN_0 &= AP_0 = IdentityMatrix[N], \\
APd &= e^{\frac{-i \cdot \delta t}{\hbar} H+C}, \\
ANd &= APd^{-1}, \\
S_0 &= R_0.
\end{aligned}
\tag{12}
$$

This results in $AN_t = e^{\frac{-i \cdot t}{\hbar} H+C}$, $AP_t = AN_t^{-1}$, $S_t = AN_t \cdot R_t \cdot AN_t^*$.

There is also a "$lindblad-eigen$" method that calculates AN_t and AP_t using the eigenvector space of the matrix $\frac{-i \cdot t}{\hbar} H + C$ each time instead of an iterative algorithm.

4.4. The *Measures* module

This model implements the two pre-defined measures, "*diagonal*" and "*entropy*", as well as a set of some helper functions.

The entropy is calculated as $\sum_i \lambda_i \cdot log(\lambda_i)$ where λ_i is the i-th eigenvalue of the supplied density matrix ρ.

Some of the helper functions are made to select the diagonal of the partial trace (to observe the behaviour of a subsystem), to calculate the partial entropy of a subsystem or the mutual entropy (for example the mutual entropy between subsystems or the mutual entropy between the photons and the excitons in the system), to measure the distance between two density matrices (to calculate the error rate or to plot a simple graph of how close did we get to the target state over time), to calculate the distance of partial trace matrices (ignoring some qubits).

4.5. The *System* module

The *System* module also contains methods to construct density matrices from the state vector or the basis state number (used by the *Experiment* module), and some helper functions to ease the creation of Hamiltonians and Lindblad/Dephasing matrices in the model.

For example, *QuantumHamiltonian* is intended to ease the creation of models that are based on qubit representation: this method accepts the total number of qubits in the system and a list of rules, each one of which consists of:

- The positions of the qubits that this rule deals with,
- The initial state,
- The target state,
- The amplitude of this rule.

For example, two rules $\{\{1,2\},\{0,1\},\{1,0\},k\}$ and $\{\{1,2\},\{1,0\},\{0,1\},k^*\}$ could be used to represent the interaction $k \cdot a_2^+ a_1^- + k^* \cdot a_1^+ a_2^-$, and one rule $\{\{5\},\{1\},\{1\},\omega\}$ could be used to represent $\omega \cdot a_5^+ a_5^-$.

A similar method *QuantumLindblad* constructs the Lindblad part of the model — the set of matrices L_i.

There are also helper methods that ease the implementation of limiting the total energy of the system (and to pass the energy limit as the parameter to the model), for example the system of 10 excitons with energy limited to 1 has only 10 basis states and Hamiltonian of size $10 * 10$, not $1024*1024$. Based on those helper methods, *QuantumHamiltonian* and *QuantumLindblad* implement an additional three-argument version, with the third argument being the definition of the subspace to which the model is limited. That argument has to be set in order to directly construct the Hamiltonian and Lindblad matrices for the reduced system — that is considerably faster than constructing the matrices for the whole system and then selecting a subspace.

5. Computation results

For all numeric experiments with input enabled the total energy was not explicitly limited, except for the natural limits imposed by the model. For numeric experiments with input disabled, the initial state has one photon and the total energy is limited to 1 (because it could not raise higher than that value).

5.1. Quantum bottleneck

Figure 4 shows the dependency of time taken to reach a target sink value on the input and output rates. It could be seen, that though the transfer speed increases with the initial increase of input and/or output rates, further increase of those rates has the effect of slowing down the transfer.

The graph has a global minimum at one point — that is the optimal (in, out) values (which are not necessarily equal to each other). Even with optimizing the input rate, the quantum bottleneck effect is observed. Also, one can observe the quantum bottleneck effect over the input rate. For any fixed *in* value there is an optimal *out* value and nice versa, and those are not constant. The graph (with the exact optimal values) also depends on the parameters of the model: μ and k, and also slightly depends on the desired target sink value, but has a similar shape.

The exact form of those dependencies is out of the scope of this paper and will be described separately.

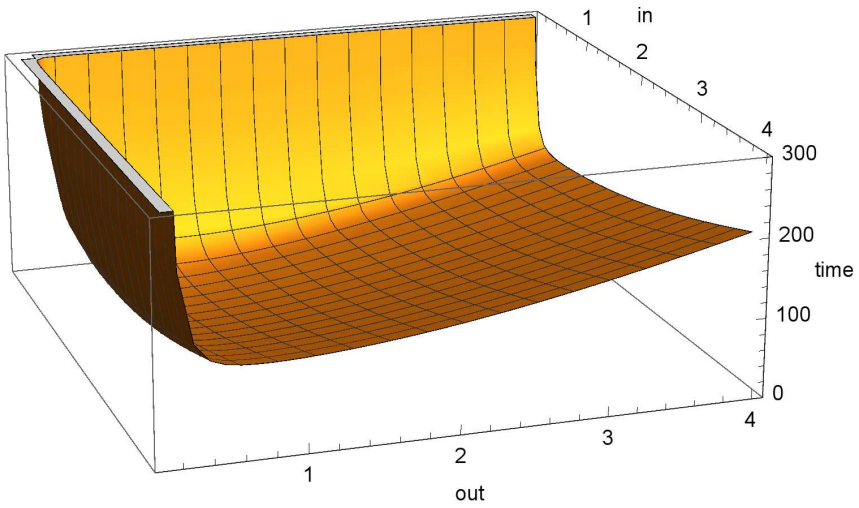

Figure 4. The dependency of time taken to reach target sink value 0.9995 over *in* and *out* rates. $\mu = 0.8$, $k = 0.5$

5.2. Dephasing-assisted transport

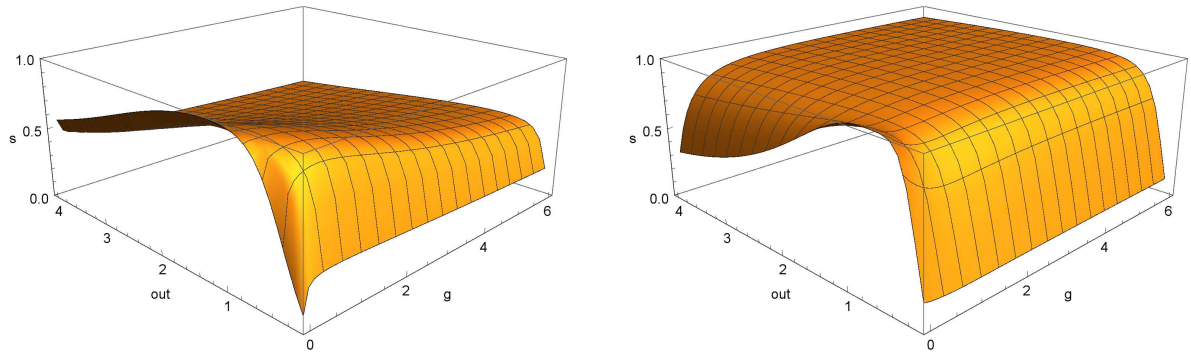

$\mu = 0.2$, $k = 0.8$, $time = 150$ $\mu = 0.8$, $k = 0.2$, $time = 60$

Figure 5. The state of sink at the fixed time. Two atoms, no input (initial state has a photon in the first cavity). Dependency over the output rate *out* and the dephasing coefficient g.

For high enough times, the absolute maximum over all possible output rates is reached when $g = 0$. But non-zero values of g can greatly improve the conductivity in cases when the output rate does not match with the optimal output rate. That is shown on figure 5. It could also be seen that the effect does not depend on g being equal to some exact value in some cases, and there is a broad range of possible values for g that improves the conductivity.

For very low times (or low target sink values, depending on the stop criterion) these graphs are different and could show other short-lived effects, but we are inspecting target sink values close to 1.0.

In the first part of figure 5 ($\mu = 0.2$, $k = 0.8$) it could be seen that non-zero values for g improve the conductivity for the case $out < outOpt$. In the second part ($\mu = 0.8$, $k = 0.2$) it could be seen that non-zero values for g improve the conductivity for the case $out > outOpt$.

The exact range of possible output rate values for which the conductivity could be improved by adding dephasing depends on the parameters of the chain.

5.3. Unitary dephasing model

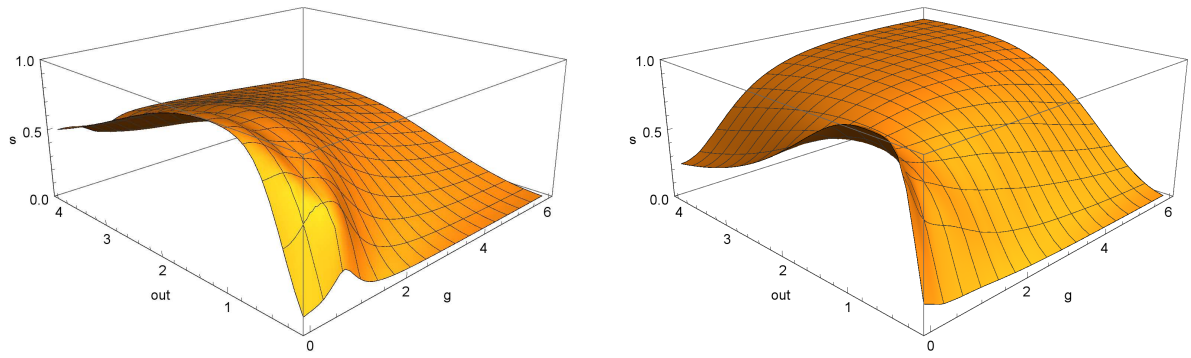

$\mu = 0.2$, $k = 0.8$, $time = 150$ $\mu = 0.8$, $k = 0.2$, $time = 60$

Figure 6. The state of sink at the fixed time. Two atoms, no input (initial state has a photon in the first cavity). Dependency over the output rate *out* and the dephasing coefficient g.

For the unitary dephasing model, the main observed effects are the same as for the Lindblad-based dephasing model in 5.2 — non-zero values of g can improve the conductivity in cases of

inoptimal values of the output rate, though the overall effect of unitary dephasing (with the supplied parameters) is milder.

Figure 6 depicts the same experiment as figure 5, but with the unitary dephasing model.

It is also worth noting that setups that were optimal to reach low target sink values (for example 0.3 or 0.4) are not always optimal to reach target sink values close to 1.

6. Conclusions

A qubit-based approach to modelling the evolution of a quantum system is described.

A description of a reusable computational model is provided, mentioning some common optimizations while still keeping the model generic — an optimized system in Hilbert space of dimension 10 with an energy limit of 1 and a system in Hilbert space of dimension 2^{10} system with the photon pumping are defined by the exact same code, and the main part of the computational system is not bound to any specific system layout at all.

Quantum bottleneck effect was explained and reproduced over both input and output rates.

Two models of dephasing showed similar results in the long term (when the numeric experiments were run long enough for the sink to reach a value close to 1).

For both dephasing models non-zero dephasing rates did not give a positive effect on the conductivity in the case of optimal output rate, but gave a large positive effect in some cases when the output rate was not optimal and when the conductivity is capped by the quantum bottleneck effect.

References

1. Breuer H., Petruccione F. The Theory of Open Quantum Systems. Oxford, 2002.
2. Kossakowski A. On quantum statistical mechanics of non-Hamiltonian systems // Rep. Math. Phys. 1972, Vol. 3, N. 4. P. 247–274.
3. Lindblad, G. On the generators of quantum dynamical semigroups // Commun. Math. Phys. 1976, Vol. 48, N. 2. P. 119–130.
4. Hou S.C., Liang S.L., Yi X.X. Non-Markovianity and memory effects in quantum open systems // Phys. Rev. A. January 2015. Vol. 91, N. 1. P. 012109.
5. Chin A.W., Rivas A., Huelga S.F., Plenio M.B. Exact mapping between system-reservoir quantum models and semi-infinite discrete chains using orthogonal polynomials // J. Math. Phys. 2010. Vol. 51. P. 092109.
6. Harpreet Singh, Arvind, Kavita Dorai Experimental protection against evolution of states in a subspace via a super-Zeno scheme on an NMR quantum information processor // Phys. Rev. A. November 2014. Vol. 90, N. 5. P. 052329.
7. Brion E., Akulin V.M., Comparat D., Dumer I., Harel G., Kebaili N., Kurizki G., Mazets I., Pillet P. Coherence protection by the quantum Zeno effect and non-holonomic control in a Rydberg Rubidium isotope // Phys. Rev. A. May 2005. Vol. 71, N. 5. P. 052311.
8. Shin-Tza Wu Quenched decoherence in qubit dynamics due to strong amplitude-damping noise // Phys. Rev. A March 2014. Vol. 89, N. 3. P. 034301.
9. Shai Machnes, Plenio M. B. Surprising Interactions of Markovian noise and Coherent Driving // URL: http://arxiv.org/abs/1408.3056
10. Mohseni M., Rebentrost P., Lloyd S., Aspuru-Guzik A. Environment-assisted quantum walks in photosynthetic energy transfer // J. Chem. Phys. 2008, Vol. 129, N. 17. P. 174106. 2008, 129, 174106.

11. Plenio M. B., Huelga S. F. Dephasing-assisted transport: quantum networks and biomolecules // New J. Phys. 2008, Vol. 10, N. 11. P. 113019.

12. Plenio M. B., Huelga S. F. Vibration, Quanta and Biology // Contemp. Phys. 2013. Vol. 54, N. 4. P. 181–207.

13. Ambainis A. Quantum walks and their algorithmic applications // Int. J. Quantum Inform. December 2003. Vol. 1, N. 4. P. 507-518.

14. Reitzner D., Nagaj D., Buzek V. Quantum Walks // Acta Physica Slovaca 2011. Vol. 61, N .6. P. 603–725.

15. Aharonov D., Ambainis A., Kempe J., Vazirani U. Quantum Walks On Graphs // Proceedings of ACM Symposium on Theory of Computation (STOC'01) July 2001. P. 50–59.

16. Childs A., Farhi E., Gutmann S. An example of the difference between quantum and classical random walks // Quant. Inf. Proc. April 2002. Vol. 1, N. 1-2. P. 35–43.

17. Fenna R. E., Matthews B. W. Chlorophyll arrangement in a bacteriochlorophyll protein from Chlorobium limicola // Nature December 1975 Vol. 258. P. 573–7.

18. Caruso F., Chin A.W., Datta1 A., Huelga S.F., Plenio M.B. Highly efficient energy excitation transfer in light-harvesting complexes: The fundamental role of noise-assisted transport // J. Chem. Phys. 2009. Vol. 131, N. 10. P. 105106.

19. Lanyon B., et al. Towards Quantum Chemistry on a Quantum Computer // Nat. Chem. January 2010. Vol. 2. P. 106–111.

20. Contreras-Pulido L.D., Bruderer M., Huelga S.F., Plenio M.B. Dephasing-assisted transport in linear triple quantum dots // New J. Phys. 2014. Vol. 16, N. 11. P. 113061.

21. Chin A.W., Huelga S.F., Plenio M.B. Coherence and decoherence in biological systems: principles of noise-assisted transport and the origin of long-lived coherences // Philosophical Transactions A August 2012. Vol. 370, N. 1972. P. 3638–3657.

22. Jaynes E.T., Cummings F.W. Comparison of quantum and semiclassical radiation theories with application to the beam maser // Proc. IEEE January 1963. Vol. 51, N. 1. P. 89–109.

23. Hubbard, J. Electron Correlations in Narrow Energy Bands // Proceedings of the Royal Society of London 1963. Vol. 276, N. 1365. P. 238–257.

24. Azuma H. Quantum computation with the Jaynes-Cummings model // Prog. Theor. Phys. 2011. Vol. 126, N. 3. P. 369–385.

25. Kok P., Munro W.J., Nemoto K., Ralph T.C., Dowling J.P., Milburn G.J. Linear optical quantum computing with photonic qubits // Rev. Mod. Phys. January 2007. Vol. 79, N. 1. P. 135–174.

26. Knill E., Laflamme R., Milburn G. J. A scheme for efficient quantum computation with linear optics // Nature January 2001. Vol. 409, P. 46–52.

27. Moiseev S.A. Off-resonant Raman echo quantum memory on atoms with natural inhomogeneous broadening in optical QED cavity // Phys. Rev. A July 2013. Vol. 88, N. 1. P. 012304.

28. Ralph T.C., White A.G., Munro W.J., Milburn G.J. Simple scheme for efficient linear optics quantum gates // Phys. Rev. A December 2001. Vol. 65, N. 1. P. 012314.

29. Toyoda K., Matsuno Y., Noguchi A., Haze S., Urabe S. Quantum Simulation of the Jaynes-Cummings-Hubbard Model Using Trapped Ions // Conference Paper, Conference on Lasers and Electro-Optics/Pacific Rim, Kyoto Japan, June 30, 2013 – July 4, 2013, ISBN: 978-1-4673-6475-1

30. Pillai C.G.S., George A.M. Excitonic thermal conduction in solids: high temperature thermal conductivity of LaCoO3 // Proc Indian Nat Sci Acad Part A September 1998. Vol. 54(5) P. 824–829.

31. Tomadin A., Fazio R. Many-body phenomena in QED-cavity arrays // J. Opt. Soc. Am. B 2010. Vol. 27, N. 6. P. A130–A136.

32. Imamoglu A., Schmidt H., Woods G., Deutsch M. Strongly Interacting Photons in a Nonlinear Cavity // Phys. Rev. Lett. August 1997. Vol. 79, N. 8. P. 1467–1470.

33. Rossini D., Fazio R. Mott-insulating and glassy phases of polaritons in 1D arrays of coupled cavities // Phys. Rev. Lett. October 2007. Vol. 99, N. 18. P. 186401.

34. Soi-Chan Lei, Tai-Kai Ng, Ray-Kuang Lee Photonic analogue of Josephson effect in a dual-species optical-lattice cavity // Opt. Express 2010. Vol. 18, N. 14. P. 14586–14597.

35. Ogryzko, V., Ozhigov, Y. Biologically inspired path to quantum computer // Proceedings of SPIE 2014. Vol. 9440, Conference on Micro and Nano Electronics, Ershovo, Moscow.

36. M.I. Makin, Jared H. Cole, Charles D. Hill, Andrew D. Greentree, Lloyd C. L. Hollenberg Time evolution of the one-dimensional Jaynes-Cummings-Hubbard Hamiltonian // Phys. Rev A 80, 043842, 2009, DOI: 10.1103, PhysRev A.80.043842.

37. Fedichkin L., Solenov D., Tamon C. Mixing and Decoherence in Continuous-Time Quantum Walks on Cycles // Quantum Information and Computation May 2006. Vol. 6, N. 3. P. 263–276.

38. Ozhigov Y., Skovoroda, N. Simulation of a relazation of electron shells in a pair of two level atoms in qubit representation // Moscow Univ. Comput. Math. Cybern., Ser. XV 2014. Vol. 38, N. 4. P. 167–173.